Author Manuscript

Author Manuscript

Author Manuscript

Author Manuscript

HHS Public Access

Author manuscript

Circ Res. Author manuscript; available in PMC 2024 March 31.

Published in final edited form as:

Circ Res. 2023 March 31; 132(7): 849–863. doi:10.1161/CIRCRESAHA.122.321938.

RNF130 Regulates LDLR Availability and Plasma LDL Cholesterol Levels

Bethan L. Clifford[1], **Kelsey E. Jarrett**[1], **Joan Cheng**[2], **Angela Cheng**[2], **Marcus Seldin**[3], **Pauline Morand**[2], **Richard Lee**[4], **Mary Chen**[5], **Angel Baldan**[5], **Thomas Q. de Aguiar Vallim**[1,2,6,7], **Elizabeth J. Tarling**[1,6,7,8,*]

[1]Department of Medicine, Division of Cardiology, University of California Los Angeles, CA, USA.

[2]Department of Biological Chemistry, David Geffen School of Medicine at UCLA, University of California Los Angeles, CA, USA.

[3]Department of Biological Chemistry, University of California Irvine, CA, USA

[4]Ionis Pharmaceuticals, Carlsbad, CA, USA.

[5]Edward A. Doisy Department of Biochemistry and Molecular Biology, Saint Louis University, St. Louis, MO, USA.

[6]Molecular Biology Institute, David Geffen School of Medicine at UCLA, University of California Los Angeles, CA, USA.

[7]Jonsson Comprehensive Cancer Center, David Geffen School of Medicine at UCLA, University of California Los Angeles, CA, USA.

[8]Lead contact

Abstract

Background: Removal of circulating plasma LDL cholesterol (LDL-C) by the liver relies on efficient endocytosis and intracellular vesicle trafficking. Increasing the availability of hepatic low-density lipoprotein receptors (LDLR) remains a major clinical target for reducing LDL-C levels. Here we describe a novel role for RNF130 in regulating plasma membrane availability of LDLR.

Methods: We performed a combination of gain- and loss-of-function experiments to determine the effect of RNF130 on LDL-C and LDLR recycling. We overexpressed RNF130 and a non-

*Correspondence: ETarling@mednet.ucla.edu.

Author Contributions

E.J.T. and T.Q. de A.V. conceived and oversaw the project. B.L.C., K.E.J., J.C., A.C., M.S., P.M., T.Q. de A.V., and E.J.T performed experiments. K.E.J. designed and purified AAV-CRISPR. B.L.C. and K.E.J. designed and performed AAV-CRISPR experiments. J.C. and A.C. assisted with animal experiments. P.M. assisted with western blotting. M.S. performed functional genomic analyses. A.B. performed FPLC lipoprotein profiles. R.L. provided antisense oligonucleotide compounds. Data analysis and statistical analyses were performed by B.L.C. and E.J.T. Figures were generated by B.L.C. and E.J.T. The manuscript was written by B.L.C. and E.J.T. All authors revised and approved the final manuscript.

Disclosures

The authors declare no conflict of interest.

Supplemental Materials

Online Figures S1–S7

Author Manuscript Author Manuscript Author Manuscript Author Manuscript

functional mutant RNF130 *in vivo* and measured plasma LDL-C and hepatic LDLR protein levels. We performed *in vitro* ubiquitination assays and immunohistochemical staining to measure levels and cellular distribution of LDLR. We supplement these experiments with three separate *in vivo* models of RNF130 loss-of-function where we disrupted *Rnf130* using either antisense oligonucleotides, germline deletion, or AAV-CRISPR and measured hepatic LDLR and plasma LDL-C.

Results: We demonstrate that RNF130 is an E3 ubiquitin ligase that ubiquitinates LDLR resulting in redistribution of the receptor away from the plasma membrane. Overexpression of RNF130 decreases hepatic LDLR and increases plasma LDL-C levels. Further, *in vitro* ubiquitination assays demonstrate RING-dependent regulation of LDLR abundance at the plasma membrane. Finally, *in vivo* disruption of *Rnf130* using antisense oligonucleotides, germline deletion, or AAV-CRISPR results in increased hepatic LDLR abundance and availability, and decreased plasma LDL-C levels.

Conclusions: Our studies identify RNF130 as a novel post-translational regulator of LDL-C levels via modulation of LDLR availability, thus providing important insight into the complex regulation of hepatic LDLR protein levels.

Graphical Abstract

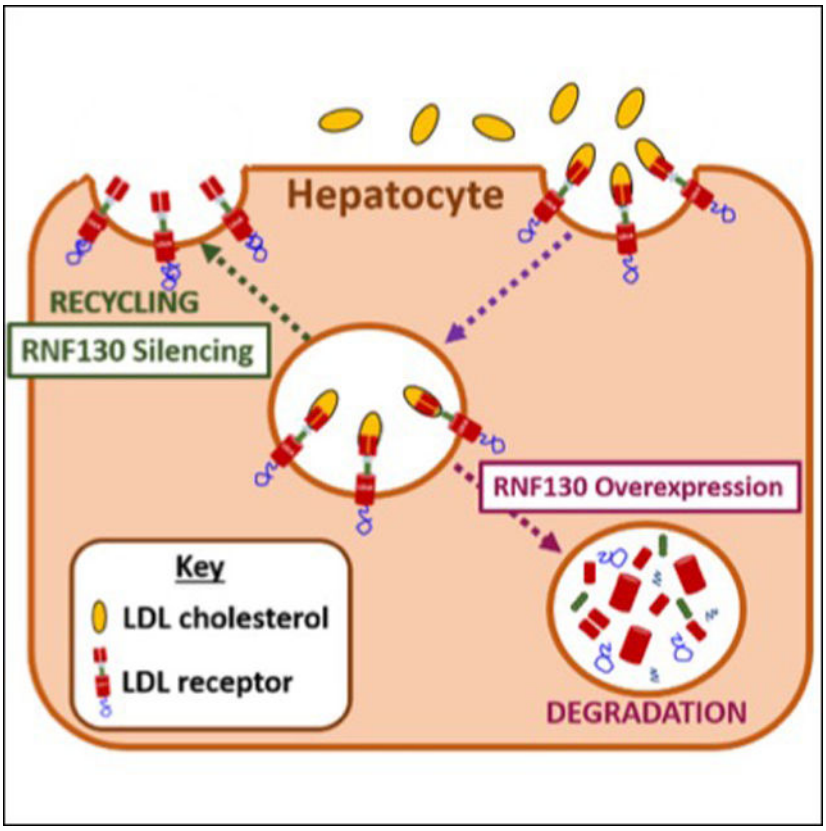

Summary Paragraph

RNF130 is a member of the unique membrane-bound protease-associated domain-containing E3 ubiquitin ligases and has no known molecular targets. Here we identify the LDLR as the

Author Manuscript Author Manuscript Author Manuscript Author Manuscript

first known target of RNF130 and show that RNF130-mediated ubiquitination of LDLR results in redistribution of the receptor away from the plasma membrane. The LDLR is the major determinant of plasma LDL cholesterol levels and we show that disruption of RNF130 expression increases hepatic LDLR abundance and decreases plasma LDL cholesterol. Our study adds a new and important layer of insight into the complex regulation of LDLR levels, which are the target of many therapeutic interventions to lower plasma LDL cholesterol.

Keywords

E3 ligase; lipids; cholesterol; LDL receptor; ubiquitin

Subject Terms:

Lipids and Cholesterol

Introduction

Elevated plasma low-density lipoprotein cholesterol (LDL-C) levels are a well-established risk factor for cardiovascular disease[1]. Plasma LDL particle concentration is regulated by the balance between synthesis and uptake from the circulation via the LDL receptor (LDLR)[2]. The liver expresses over 70% of whole body LDLR and is the major determinant of plasma LDL-C concentrations[3,4]. As such, regulation of LDLR is complex and under tight control by multiple pathways.

RNF130, also known as GOLIATH, is the mammalian homolog of the *Drosophila* protease-associated (PA) domain-containing E3 ligase Goliath (*dGoliath*). E3 ligases are part of the cellular ubiquitin system that not only controls the selective degradation of proteins by the 26S proteasome, but can also modify proteins and regulate their cellular localization[5]. E3 ligases catalyze transfer of ubiquitin to the target protein, thereby conferring specificity and regulation to these processes. Most E3 ligases are cytosolic, presumably to increase their exposure to substrates, E2 conjugating enzymes, and ubiquitin, thus allowing for rapid modification and regulation of target proteins. Despite there being over 600 RING E3 ligases[6], only a small number, that includes RNF130, contain a *bona fide* transmembrane domain (TMD)[7]. The function and molecular targets of RNF130 are unknown[8,9].

RNF130, like the other members of the PA domain-containing E3 ligase sub-family, exhibits a distinct domain architecture, consisting of a signal peptide, a PA domain, a TMD, and a RING (Really Interesting New Gene) domain[10]. Ubiquitination events mediated by *Drosophila* Goliath family members have been shown to regulate specific cellular events such as endocytosis[7,11] and protein-protein interactions[12,13]. Given the highly conserved structural architecture between RNF130 and other PA-TM-RING proteins, we hypothesized that RNF130 may play a role in the endocytic recycling of membrane receptors.

In the present study we identify RNF130 as a novel post-translational regulator of hepatic LDLR and plasma LDL-C levels. Using a combination of molecular, biochemical, and *in vivo* metabolic analyses, we have determined that RNF130 ubiquitinates the LDLR, reduces

Author Manuscript Author Manuscript Author Manuscript Author Manuscript

plasma membrane LDLR localization and LDL uptake, and increases plasma LDL-C levels. We also demonstrate, using three different independent *in vivo* approaches, that loss of RNF130 in mice results in increased hepatic levels of LDLR and reduced plasma LDL-C levels. We propose that RNF130 allows for the modulation of LDLR endocytosis and/or recycling, and therefore the regulation of available LDLR molecules at the cell surface.

Methods

Data Availability.

The authors declare that all supporting data are available within the article and its online supplementary files.

Mice, diets, and treatments.

Wildtype C57BL/6 mice were purchased from The Jackson Laboratory (JAX, #00664). *Ldlr*$^{-/-}$ and *Pcsk9*$^{-/-}$ mice on a C57BL/6 background were originally purchased from The Jackson Laboratory. Mice with a targeted disruption of *Rnf130* were generated using embryonic stem cells from the European Conditional Mouse Mutagenesis program (EUCOMM) and the European Mouse Mutant Cell Repository (EuMMCR) with a knockout-first, conditional-ready cassette targeting exon 3 of *Rnf130*. To obtain germline transmission of the *Rnf130* KO-first Tm1a allele (*Rnf130*$^{KO1\text{-}Tm1a}$) on a C57BL/6 background, *Rnf130*$^{KO1\text{-}Tm1a}$ ES cells were injected into blastocysts and the resulting chimeras were bred with C57BL/6 mice. Germline transmission was confirmed by PCR genotyping for a minimum of ten litters. All animals were maintained on normal rodent diet (Ralston Purina Company, 5001) at UCLA on a 12-hour/12-hour light/dark cycle with unlimited access to food and water. All animals used in the study were male mice 8–10 weeks of age. As adenovirus and AAV transduction is known to be different between male and female mice, only male animals were used[14]. Animals were randomly assigned to control or treatment groups. Human RNF130 was cloned as described below and shuttled into adenoviral expression vectors. Adenovirus particles were prepared using the AdEasy system (Agilent) and purified by Cesium Chloride (CsCl) gradient centrifugation. The virus was dialyzed for 48 hours and stored at −80°C. Particles were quantified by serial dilution methods by detection of plaques in HEK293Ad (Agilent) cells. Adenovirus (10^9 PFU) was delivered by tail-vein injection. Mice were treated with a single injection of either control adenovirus, or adenovirus expressing wildtype or mutant RNF130 on day 0, as indicated in the figure legend, and mice were sacrificed 7 days later. The plasmids required for the manufacture of adeno-associated virus (AAV), pAdDeltaF6 adeno helper plasmid (PL-F-PVADF6) and pAAV2/8 (PL-T-PV0007), were obtained from the University of Pennsylvania Vector Core. AAV was prepared by the triple-transfection method[15] in HEK293T cells (ATCC, CRL-3216) and purified by CsCl gradient as previously described[16]. Aliquots of concentrated virus were stored at −80°C until injection. Viral titers were determined by qPCR following DNase digestion and normalized to a standard curve of known genome copies. AAV (5×10^{11} genome copies) was delivered by intraperitoneal injection. A guide RNA sequence specific to *Rnf130* was used to target mouse *Rnf130* by CRISPR/Cas9 (5’gactgcacagtgatcgaagt). Gen. 2.5 16-mer antisense oligonucleotides (ASO) targeted to mouse *Rnf130* (5’attctgttatcatgac) or control sequences were synthesized and purified by

Author Manuscript Author Manuscript Author Manuscript Author Manuscript

Ionis Pharmaceuticals (Carlsbad, CA). ASOs were delivered by intraperitoneal injection twice weekly at a dose of 25 mg/kg for 4 weeks (as described in the figure legends).

Analysis of CRISPR-based gene disruption

Liver genomic DNA was isolated using the Qiagen DNeasy kit. DNA (100ng) was subjected to qPCR using primers specific to the AAV-Control and AAV-gRNA vectors to assess the relative amount of virus present in the liver. A standard curve from plasmids used for virus production was used to quantify AAV genomes per μg of DNA.

Off-target sites for *Rnf130* guide RNA were determined using the online bioinformatics tool, COSMID at https://crispr.bme.gatech.edu/ as previously described[16]. For on-target editing, 50 μg cDNA was amplified using primers surrounding the gRNA target site. The resulting band was gel purified (Clontech) and sequenced by Sanger Sequencing. Editing efficiency was estimated using Synthego ICE (Inference of CRIPSR Edits; https://www.biorxiv.org/content/early/2019/01/14/251082).

Plasma analysis.

HDL and LDL/VLDL fractions were separated using a manganese chloride-heparin precipitation[17]. Subsequent fractions and total cholesterol were measured using a colorimetric assay (Infinity Cholesterol Reagent; Thermo Scientific). Plasma cholesterol lipoprotein profiles were determined from individual mice using the modified CLiP method as previously described[18,19]. Lipoprotein profiles are plotted as mean absorbance unit (AU) ±SEM for all animals in each treatment group.

RNA analysis.

Liver tissue was homogenized, and total RNA extracted using QIAzol reagent (Invitrogen Life Technologies). 500ng total RNA was reverse transcribed using the High Capacity cDNA Reverse Transcriptase Kit (Applied Biosystems) and gene expression determined using a Lightcycler480 Real-time qPCR machine and SYBR-Green mastermix (Roche). Relative gene expression was determined using an efficiency corrected method and efficiency was determined from a 3-log serial dilutions standard curve made from cDNA pooled from all samples. Results were normalized to *36b4* mRNA. Primer sequences are available upon request.

Protein analysis.

Liver tissue was homogenized, and protein extracted using RIPA buffer with protease inhibitor cocktail mix (1 Complete MINI EDTA-free protease inhibitor tablet (Roche), 25 μg/mL calpain inhibitor (Sigma), and 200 μM PMSF (Sigma)). 25–50 μg protein was separated on an SDS-PAGE gel (BioRad) and transferred to a polyvinylidene fluoride membrane. Membranes were incubated overnight with antibodies to EGFR (1:1,000; Invitrogen), FLAG (1:1,000; Sigma), RNF130 (1:1000; Novus Biologicals), GFP (1:1,000; Santa Cruz Biotechnology), HA.11 (1:1,000; Covance), LDLR (1:1,000; Cayman), LRP1 (1:1,000; Abcam), PDI (1:1,000; Cell Signaling), and Transferrin Receptor (1:1,000; Invitrogen). Proteins were detected with HRP-conjugated secondary antibodies (1:10,000;

Author Manuscript Author Manuscript Author Manuscript Author Manuscript

GE Healthcare) and visualized using an AI600 Imager (GE Healthcare). Densitometry analysis was performed using ImageQuant (TL 8.1, GE Healthcare).

Plasmids and expression constructs.

The pDEST47-hLDLR and K1/6/20RC29A mutant plasmids were a kind gift from Dr. Peter Tontonoz[20,21]. The pcDNA3.1-(HA-Ubiquitin)$_6$ plasmid was a gift from Dr. James Wohlschlegel (UCLA, USA). Human RNF130 was amplified (Fwd 5' atgagctgcgcggggcgggcgggccctgccc; Rev 5' gcttgaatgctaatgaggtagaatggttttga) from Hep3B cell cDNA using HiFi DNA polymerase (KAPA Biosciences). Human RNF130 was also generated with a 3xFLAG epitope engineered at amino acid position 28 after the signal peptide as a double-stranded DNA gBlock (IDT Technologies). Additionally, the C304A mutation was introduced into the RING domain of RNF130. Restriction digests and DNA sequencing were used to confirm all constructs used in this study. For adenoviral studies, full length human RNF130 was sub-cloned from pcDNA3.1 into the pAd-CMV vector.

Guide RNA Design

Staphylococcus aureus guide RNAs (gRNAs) targeting murine *Rnf130* were designed by examining the coding sequence using SnapGene. Preliminary off target prediction was completed using CRISPR Off-target Sites with Mismatches, Insertions and/or Deletions (COSMID)[22]. The search terms used for the off-target search aimed to return the highest possible number of off-targets, using a NNGRR protospacer adjacent motif (PAM) instead of NNGRRT, and allowing three mismatches and two insertions or deletions within the gRNA and PAM sequence. Of the available gRNAs, we selected, cloned, and tested the gRNAs with the fewest predicted off-targets. The plasmid 1313 pAAV-U6-BbsI-MluI-gRNA-SA-HLP-SACas9-HA-OLLAS-spA (Addgene #109304) was a gift from Dr. William Lagor at Baylor College of Medicine[23]. This AAV vector backbone contains inverted terminal repeats surrounding a U6 promoter driving gRNA expression and a hybrid liver-specific promoter (HLP) driving expression of *Staphylococcus aureus* Cas9 (SaCas9). The gRNA was cloned into this vector by ligating annealed oligos matching the desired gRNA sequence into the BbsI cloning site behind the U6 promoter. The Control AAV-CRISPR used in experiments is the parent vector containing the BbsI cloning site. When the sequence including the BbsI site is queried using COSMID for the SaCas9 NNGRR PAM, no possible off-targets are returned.

Cell culture and transfection.

HEK293T, Hep3B, and HepG2 cells were obtained from ATCC (CRL-3216, HB-8064, HB-8065). Cells were maintained in DMEM containing 10% FBS. For transfections, cells were plated onto cell-culture-treated plates or coverslips (Corning) at 60% confluence on Day 0. Cells were transfected with a total of 1μg combined DNA plasmids using FuGENEHD (Promega) according to the manufacturer's instructions. After 24–48hr incubation, cells were collected for downstream processing (western blot, immunoprecipitation) or fixed and mounted for imaging. Quantification of confocal images was performed using ImageJ.

Author Manuscript Author Manuscript Author Manuscript Author Manuscript

Cell Surface Biotinylation.

For cell surface biotinylation, HEK293T cells were transfected with plasmids encoding GFP-tagged LDLR, HA-tagged ubiquitin, and N-terminally FLAG-tagged WT or mutant (C304A) RNF130 as described above. After 36 hours, cells were washed in PBS++ (Phosphate buffered saline with 0.02mM $CaCl_2$ and 0.15mM $MgCl_2$) and then incubated for 30 minutes on ice with EZ-link SulfoNHS-SS Biotin (diluted in PBS++). The cells were washed in PBS++ and the reaction was quenched for 30 minutes at 4°C in quenching buffer (PBS++ with 100mM glycine). Biotin-modified proteins were immunoprecipitated with NeutrAvidin streptavidin beads overnight at 4°C. The following day, biotin-modified proteins were collected by centrifugation at 5,000 × g for 5 min at 4°C. Intracellular, unmodified proteins were collected from the supernatant of the 5,000 × g spin. The streptavidin beads were washed three times in PBS++ before proteins were removed from the beads by incubation at 42°C for 20 min in Laemmli sample loading buffer supplemented with β-mercaptoethanol. Equal % volume of individual fractions were subject to immunoblotting.

Immunoprecipitation.

Cells were plated and transfected as described above. Total cell lysates were prepared in RIPA buffer as described above. Lysates were cleared by centrifugation at 4°C for 10 min at 10,000 × *g*. Protein concentration was determined using the BCA Assay (BioRad) with bovine serum albumin as a reference. To immunoprecipitate LDLR-GFP, equal amounts of protein of cleared lysate were incubated with anti-GFP polysera (1:1,000) overnight prior to addition of protein-G agarose beads (Santa Cruz Biotechnology) for an additional 2 hr. Subsequently, beads were washed 3x with RIPA buffer supplemented with protease inhibitors. All incubations and washes were done at 4°C with rotation. Proteins were eluted from the beads by incubating in Laemmli sample buffer at 70°C for 30 min.

DiI-LDL Uptake Assay.

Cells were plated on coverslips and transfected as above. After 24 hr, cells were treated with 50 μg/mL diI-LDL (3,3'-dioctadecylindocarbocyanine-low density lipoprotein) for 30 min at 4°C. Subsequently, cells were placed at 37°C for 4 hours prior to fixation. After 4 hr, cells were washed, fixed in 4% PFA for 15 min, and coverslips mounted onto slides before imaging using a 63X lens under immersion oil. Images were captured using a Zeiss AxioCam 506 camera and post-image analysis and quantification was carried out using ImageJ.

Imaging.

Cells were plated and transfected as described above. At harvest, cells were washed, fixed in 4% PFA for 15 min, and then washed again before briefly being stored in PBS. Coverslips were mounted on to slides and imaged using a 63X lens under immersion oil. Images were captured using a Zeiss AxioCam 506 camera and post-image analysis and quantification was carried out using ImageJ. Images from three independent replicate experiments were analyzed and quantified. Representative images were chosen that best illustrated the mean/average of the quantification.

Author Manuscript Author Manuscript Author Manuscript Author Manuscript

Statistical Analysis.

Statistical analysis was performed using Prism Graphpad software (V8.0). All results are reported as mean ± SEM, as stated in the figure legends. A $P \leq 0.05$ was considered significant and statistical significance is shown as described in the figure legends. Gaussian distribution was determined using the Shapiro-Wilk normality test for sample size n>6. Data determined to be parametric were analyzed by unpaired two-tailed Student's *t*-test to compare two independent groups or by two-way ANOVA followed by Tukey's HSD post-hoc multiple comparison analysis for more than two groups. Data determined to be non-parametric were analyzed by Mann-Whitney U-test for comparison of two groups and Kruskal-Wallis test with post-hoc Dunn's test for comparison of more than two groups. For sample size n<6, non-parametric tests (Mann-Whitney U-test for comparison of 2 groups and Kruskal-Wallis with Dunn's correction for comparison of more than 2 groups) were used. Outliers were determined using the ROUT outlier test with an FDR of 1%. Additionally, animals were removed from analyses due to attrition from in vivo studies because of excessive weight loss (>20% body weight), or noted mis-injects of adenovirus, AAV, or ASO.

Study Approval.

All animal experiments were approved by the Office of Animal Research Oversight (OARO) and the Institutional Animal Care and Use Committee (IACUC) at the University of California Los Angeles.

Results

RNF130 expression decreases hepatic LDLR levels.

Members of the *Rnf130* family of protease-associated (PA) domain E3 ligases have previously been implicated in the regulation of endocytic recycling events[7]. To determine whether RNF130 is also localized to endocytic compartments, we transfected HEK293 and HepG2 cells with plasmids encoding a GFP-tagged endosomal marker (Rab27-GFP) and an N-terminally FLAG-tagged human RNF130. Since the coding sequence for RNF130 contains a predicted signal peptide (amino acids 1–27), and addition of a tag on the carboxy-terminal end of the protein renders it non-functional (data not shown), we engineered a 3xFLAG-tag immediately after the signal peptide. Similar to other *Rnf130* family members including *Drosophila* Godzilla^{CG10277} and human RNF167, we observed that RNF130 was localized to punctate vesicular structures that co-localized with Rab27, a marker of endosomal compartments (Fig. 1A), suggesting RNF130 may also play a role in regulating endocytic events.

Using a panel of tissues isolated from C57BL6/J mice we determined that *Rnf130* is most highly expressed in liver, adipose, and brain, with ubiquitous expression in other tissues (Fig. S1A). To understand the effects of modulating RNF130 expression on endocytosis *in vivo*, we generated adenovirus particles to overexpress human RNF130 in the livers of mice. Wildtype (WT) mice were injected once on day 0 with either control adenovirus (Ad-Ctr) or adenovirus expressing human RNF130 (Ad-RNF130) and tissues harvested 7 days later (Fig. 1B). To determine whether RNF130 grossly affected endocytosis we first measured

Author Manuscript Author Manuscript Author Manuscript Author Manuscript

the levels of endocytosed receptors. To our surprise, overexpression of RNF130 (Fig. 1C) significantly decreased levels of LDLR (Fig. 1D–E), without changing the levels of other endocytosed receptors, EGFR, Transferrin receptor (TfR), LDLR-related protein 1 (LRP-1), suggesting some specificity for the regulation of LDLR. Changes in LDLR protein (Fig. 1D–E) were also independent of any change in *Ldlr* mRNA levels (Fig. 1F), suggesting RNF130 regulates LDLR levels via a post-transcriptional mechanism.

Since hepatic LDLR is the major determinant of circulating plasma LDL-C levels, we also measured levels of plasma lipids. RNF130 overexpression resulted in significantly increased total (Fig. 1G) and non-HDL (LDL/VLDL) plasma cholesterol levels (Fig. 1H). FPLC analysis of plasma samples from individual mice demonstrated a significant increase in the LDL-C fraction (Fig. 1I). In contrast, plasma TAG and HDL-C levels were either modestly decreased (Fig. S1B) or unchanged (Fig. S1C).

RNF130 is a RING-dependent E3 ligase that ubiquitinates LDLR and redistributes LDLR away from the plasma membrane

We next sought to determine the molecular mechanism underlying the regulation of LDL-C by RNF130. Like other members of the *Rnf130* family, RNF130 has been reported to function as an E3 ubiquitin ligase[8]. Therefore, we hypothesized that LDLR may be ubiquitinated by RNF130. To test this hypothesis, we transfected HEK293 cells with plasmids encoding GFP-tagged LDLR, HA-tagged ubiquitin, and, where indicated, an N-terminally FLAG-tagged human RNF130. As shown in Fig. 2A, total LDLR protein was decreased in cells co-expressing RNF130 (Fig. 2A; Input) which was accompanied by greatly increased ubiquitination of LDLR (Fig. 2A; Ubiquitination).

LDLR has multiple highly conserved potential ubiquitination sites within its cytoplasmic tail (Lys^{811}, Lys^{816}, Lys^{830}, and Cys^{839}). We repeated the experiments described above but using an LDLR construct where these four residues were mutated to arginine or alanine, respectively. Combined mutation of all four residues (K811/816/830R/C839A) prevented both ubiquitination of LDLR (Fig. 2B; Ubiquitination) and the loss of LDLR-GFP protein (Fig. 2B; Input). Consistent with our *in vivo* observations (Fig. 1D), overexpression of RNF130 had no effect on levels of additional endocytosed receptors EGFR, TfR, and the related lipoprotein receptor LRP-1 (Fig. S2A), further supporting that this ubiquitination event is specific to LDLR and not a gross change in receptors known to be internalized via clathrin-mediated endocytosis.

Having determined that RNF130 requires specific residues in the cytoplasmic tail of LDLR to be intact for a ubiquitination event, we next turned to assessing whether the E3 ubiquitin ligase function of RNF130 was essential for this observation. The catalytic domain required for ubiquitination activity of RING E3 ligases is the RING domain and specific mutations in this domain have been shown to impair ubiquitination of target proteins[6,24]. RNF130 containing a single point mutation in the RING domain ($Cys^{304} \rightarrow Ala^{304}$) failed to ubiquitinate LDLR (Fig. 2C; Ubiquitination) or lower LDLR protein levels (Fig. 2C; Input). Further, the levels of FLAG-tagged RNF130 were elevated when the RING domain was mutated, compared to wildtype RNF130 (Fig. 2C; Input) with no significant difference in *RNF130* mRNA expression (Fig. S2B), suggesting that RNF130 can also catalyze its own

Author Manuscript Author Manuscript Author Manuscript Author Manuscript

ubiquitination and degradation. Such self-ubiquitination is in agreement with previously published reports of RNF130[8,9] and other RING E3 ligases.

A significant percent of LDLR protein is normally expressed at the cell surface which is important for its function in the endocytic pathway that internalizes LDL-C particles[25]. To determine whether RNF130 affects LDLR abundance at the cell surface, we transfected HEK293 cells with plasmids encoding GFP-tagged LDLR, HA-tagged ubiquitin, and N-terminally FLAG-tagged WT or mutant (C304A) RNF130. Transfected cells were exposed to biotin to label cell surface proteins before quenching the reaction to prevent subsequent modification of intracellular proteins released after cell lysis. As expected, WT FLAG-RNF130 but not mutant FLAG-RNF130^{C304A}, reduced GFP-tagged LDLR protein levels in whole cell lysates (Fig. 2D; IB:GFP lanes 2–4). WT RNF130 decreased the abundance of GFP-tagged LDLR at the cell surface (Fig. 2D; IB:GFP lane 7 *vs.* 6). In contrast, levels of GFP-LDLR were not reduced in cells following co-expression of mutant RNF130^{C304A} (Fig. 2D; IB:GFP lane 8 *vs.* 6), consistent with the inability of mutant RNF130^{C304A} to degrade LDLR. Analysis of intracellular LDLR levels indicated that there was no change in intracellular LDLR levels following co-expression of WT RNF130 (Fig. 2D; IB:GFP lane 11 *vs.* 10). Together, these data suggest that WT RNF130 has proportionally greater effects on LDLR abundance at the cell surface.

In addition to signaling for degradation in the proteasome, protein ubiquitination can also serve as an internalization signal for specific proteins at the plasma membrane[7,26]. As effects of RNF130 on LDLR protein levels were greater at the cell surface, we hypothesized that the ubiquitination of LDLR by RNF130 may result in redistribution of LDLR away from the cell surface, in addition to possibly increasing degradation of LDLR. Immunocytochemical staining showed that co-expression of RNF130 dramatically decreased the levels of LDLR at the cell surface (Fig. 2E; middle panel). Although there was still LDLR present in intracellular compartments (Fig. 2E; middle panel), quantification of mean fluorescent intensity demonstrated a significant reduction in GFP fluorescence indicating that total levels of GFP-tagged LDLR were also decreased with co-expression of RNF130 (Fig. 2F). In contrast to WT RNF130, cells expressing mutant RNF130^{C304A} continued to express high levels of LDLR both at the cell surface and in intracellular compartments (Fig. 2E; right panel and Fig. 2F). Additionally, levels and localization of mutant LDLR-GFP (MUT-LDLR-GFP) were unchanged in cells expressing WT RNF130 (Fig. S2C–D).

The data of Fig. 2D–F demonstrate that RNF130-mediated ubiquitination of LDLR results in the redistribution of LDLR away from the plasma membrane. We next used immunocytochemical staining to ask what intracellular compartments LDLR is redistributed to. These studies demonstrated that LDLR is redistributed to intracellular vesicles that co-localize with NPC-1, a marker of late endosomes and lysosomes (Fig. S2E), consistent with lysosomal degradation of LDLR. We also probed the degradative mechanism that occurs using inhibitors of proteasomal degradation. Consistent with previous findings that LDLR degradation occurs in the lysosome, the proteasome inhibitor MG132 stabilized RNF130 protein, but did not stabilize LDLR (Fig. S2F). Finally, we asked whether RNF130-mediated ubiquitination of LDLR affects uptake of LDL particles. We co-transfected HepG2 cells with LDLR-GFP and either control plasmid or plasmid expressing WT RNF130. Following

Author Manuscript Author Manuscript Author Manuscript Author Manuscript

transfection, cells were incubated in the presence of diI-LDL particles to determine LDL uptake. These studies demonstrated that LDL uptake was significantly reduced in cells expressing RNF130, likely as a consequence of RNF130-mediated LDLR ubiquitination and redistribution away from the plasma membrane (Fig. S2G–H).

E3-Ligase activity of RNF130 is required for the regulation of hepatic LDLR and plasma LDL-C.

To assess whether the E3 ubiquitin ligase function of RNF130 was required for its ability to increase plasma LDL-C *in vivo*, we treated WT mice with either control or adenovirus overexpressing FLAG-tagged WT RNF130 or RNF130 containing the C304A point mutation in the RING domain (Fig. 3A). Consistent with previous studies (Fig. 1), FLAG-RNF130 overexpression in WT mice (Fig. S3A–B) increased total and LDL cholesterol levels (Fig. 3B–C) and this was associated with a decrease in LDLR protein (Fig. S3A, C). In contrast, expression of mutant RNF130^{C304A} (Fig. S3A–B) failed to alter plasma cholesterol levels (Fig. 3B–C) or LDLR protein (Fig. S3A, C). Collectively, these experiments together with the data of Fig. 2, demonstrate that RNF130 regulates LDL-C through its function as a ubiquitin ligase, and that the consequence of this ubiquitination is likely a combination of redistribution of LDLR from the plasma membrane and degradation of LDLR protein.

To determine if the RNF130-mediated increase in LDL-C is dependent on the presence of hepatic LDLR, we overexpressed RNF130 in LDLR knockout (*Ldlr*$^{-/-}$) mice (Fig. 3D). Overexpression of RNF130 (Fig. S3D) in *Ldlr*$^{-/-}$ mice did not change plasma total cholesterol (Fig. 3E, F), LDL/VLDL-C (Fig. 3F, Fig. S3E), HDL-C, or TAG levels (Fig. S3F–G), demonstrating that LDLR is required for the RNF130-dependent increase in LDL-C levels *in vivo*.

Efficacy of RNF130-mediated regulation of plasma cholesterol levels is dependent on hepatic LDLR abundance

Based on these data, we hypothesized that overexpression of RNF130 may have more potent effects on plasma LDL-C in mouse models that exhibit elevated endogenous levels of hepatic LDLR protein compared to WT mice.

We overexpressed RNF130 in *Pcsk9*$^{-/-}$ mice, a model of increased hepatic LDL receptors[27,28]. PCSK9 normally binds to the LDLR/LDL-C complex as it is being internalized and signals for the LDLR to be degraded in the lysosome, instead of being recycled back to the plasma membrane[29]. Consequently, compared to *Pcsk9*$^{+/+}$ mice, *Pcsk9*$^{-/-}$ mice have elevated levels of hepatic LDLR protein and significantly reduced levels of plasma LDL-C[28]. Overexpression of RNF130 in *Pcsk9*$^{-/-}$ mice (Fig. 4A–B) resulted in increased plasma total cholesterol (Fig. 4C, 4E), LDL/VLDL-C (Fig. 4D–E), and HDL-C levels (Fig. S4A), with no change in plasma TAG levels (Fig. S4B). Consistent with data from WT mice (Fig. 1E–F), in the absence of any change in *Ldlr* mRNA (Fig. 4F), RNF130 overexpression resulted in significantly decreased LDLR protein levels (Fig. 4G).

Together these data show that overexpression of RNF130 in WT and *Pcsk9*$^{-/-}$ mice increased LDL/VLDL-C levels by 36% (Fig. 1H–I) and 70% (Fig. 4D–E), respectively,

Author Manuscript Author Manuscript Author Manuscript Author Manuscript

suggesting that the efficacy of RNF130 for increasing LDL/VLDL-C is enhanced when basal hepatic LDLR levels are elevated. Together with data from Figure 2, these data demonstrate that overexpression of RNF130 increases plasma LDL-C by a process dependent on both the expression and availability of hepatic LDLR.

Partial knockout of *Rnf130* in mice results in increased hepatic LDLR and reduced plasma cholesterol

Thus far, we have shown that RNF130 gain-of-function results in reduced hepatic LDLR and increased plasma LDL-C levels. To carry out the reverse loss-of-function, we first generated mice with a targeted disruption of *Rnf130* (Fig. S5A; Tm1a allele). Germline transmission was confirmed by PCR genotyping (Fig. S5B) for a minimum of ten litters[30]. These "knockout-first, conditional-ready" mice have the potential to generate global knockout animals (Fig. S5A; Tm1b allele) by crossing with mice expressing Cre recombinase or conditional-ready animals with a floxed allele (Fig. S5A; Tm1c allele) by crossing with mice expressing Flp recombinase. We attempted to generate mice with both Tm1b and Tm1c alleles (Fig. S5A). However we were unable to obtain any mice with the correct genotype. Upon sequencing of the ES cells used to generate the Tm1a mice (Fig. S5A), we discovered that the downstream loxP site (Fig. S5A; solid red triangle) required for these recombination events was not present in any of the clones analyzed, thus explaining the lack of Tm1b and Tm1c mice. We therefore proceeded to investigate the loss of *Rnf130* function *in vivo* using our knockout-first Tm1a allele mice (Fig. S5A–B).

When heterozygous $Rnf130^{+/-}$ Tm1a mice were crossed with one another, pups were obtained at the ratio of 1 $Rnf130^{+/+}$: 2 $Rnf130^{+/-}$: 0.6 $Rnf130^{-/-}$ (n=35 litters, 204 pups total, mean litter size 5.8 pups per litter) which differs from the expected Mendelian ratio of 1:2:1 (Fig. 5A), suggesting that homozygous deletion of *Rnf130* is not well tolerated. We next investigated the phenotype of the $Rnf130^{-/-}$ mice that survived birth. Surviving $Rnf130^{-/-}$ Tm1a pups were able to nurse, feed, and mature into adults, and the body weight of adult mice at 10 weeks of age was not significantly different from either heterozygous ($Rnf130^{+/-}$) or wildtype ($Rnf130^{+/+}$) mice (Fig. S5C). Gene expression analysis of livers from $Rnf130^{+/+}$, $Rnf130^{+/-}$, and $Rnf130^{-/-}$ mice demonstrated that $Rnf130^{-/-}$ mice had 30% residual *Rnf130* mRNA expression (Fig. 5B), suggesting that surviving hypomorphic mice have escaped entire loss of *Rnf130*. Expression analysis of predicted *Rnf130* transcripts and the knockout cassette indicate that a truncated mRNA is not the reason for the 30% residual *Rnf130* expression (Fig. S5D–F). Furthermore, $Rnf130^{+/-}$ mice only experienced a 30% knockdown of mRNA expression, significantly lower than the 50% that would be expected of heterozygous animals (Fig. 5B). We also asked what happened to *Rnf130* expression in other tissues in which *Rnf130* is also highly expressed, such as the brain (Fig. S1A). Gene expression analysis of *Rnf130* (Fig. S5G), its predicted transcripts (Fig. S5H–I), and the knockout cassette (Fig. S5J) also demonstrated that $Rnf130^{-/-}$ mice had 30% residual *Rnf130* mRNA expression in the brain.

Given the observed partial knockdown of *Rnf130* mRNA (Fig. 5 and Fig S5C–J), we next wanted to determine what happened to RNF130 protein expression in these mice. We tested

Author Manuscript Author Manuscript Author Manuscript Author Manuscript

all commercially available antibodies to mouse RNF130 and found that none were specific for endogenous mouse RNF130 (Fig. S5K–O).

Nevertheless, importantly plasma lipid analysis in *Rnf130*$^{-/-}$ mice showed a significant reduction in circulating plasma total cholesterol (Fig. 5C) and these changes appeared to be present in the LDL fraction (Fig. 5D). Consistent with such a decrease in plasma LDL-C, there was a concomitant increase in LDLR protein expression in *Rnf130*$^{-/-}$ mice compared to their wild-type littermates (Fig. 5E).

Liver-specific disruption of *Rnf130* reduces plasma cholesterol levels

Given that hepatic LDLR levels have a major role in regulating clearance of LDL-C from the circulation, we next sought to determine whether acute reductions in RNF130 in the livers of adult mice reduced plasma LDL-C levels. We used an all-in-one AAV-CRISPR vector expressing a small guide RNA (gRNA) targeting exon 5 of *Rnf130*, and Cas9 from *Staphylococcus aureus* (SaCas9) (Fig. S6A). We targeted exon 5 because exon 5 encodes the RING domain, which is critical for RNF130 function (Fig. 2–3). The CRISPR system was packaged into AAV 2/8 which has a high tropism for liver[31,32], and we increased liver-specificity further by expressing SaCas9 under the control of a liver-specific promoter (Fig. S6A). C57BL/6 mice were assigned into groups and blood samples drawn to ensure equivalent levels of plasma cholesterol at baseline (Fig. S6B).

Mice were injected once on day 0 with either control AAV-CRISPR or *Rnf130* AAV-CRISPR (Fig. 6A) at a dose of 5×10^{11} genome copies per animal. After two weeks, there was no significant difference in body weight between animals treated with either control AAV-CRISPR or *Rnf130* AAV-CRISPR (Fig. S6C). Hepatic *Rnf130* mRNA expression was decreased by 70% in mice treated with *Rnf130* AAV-CRISPR (Fig. 6B). To ensure comparable viral load had been achieved in both groups, we performed PCR to amplify within SaCas9 (Fig. S6D) and measured viral genome copies by qPCR (Fig. S6E). These data confirm that viral loads were similar in both groups. To confirm the decreases seen in *Rnf130* mRNA were the consequence of CRISPR-mediated gene disruption, we sequenced samples from control- and *Rnf130*-AAV-CRISPR treated animals and performed editing analyses using Synthego ICE. As expected, we detected INDELs in *Rnf130* exon 5 in mice treated with *Rnf130* AAV-CRISPR (Fig. S6F). These analyses also show increased values for discordant sequences in these mice when compared to control treated animals (Fig. S6G), suggesting some INDELs are affecting an area larger than the 8bp measurement window. Together, these data indicate that a proportion of the remaining mRNA is disrupted, and that the observed decrease in *Rnf130* mRNA levels are the consequence of CRISPR gene editing. We also wanted to determine effects on RNF130 protein levels following AAV-CRISPR-mediated disruption of *Rnf130* mRNA. As in Fig. S5, we repeated our protein analysis using all commercially available antibodies in the livers of mice treated with either control- or *Rnf130*-AAV-CRISPR and found that none were specific for endogenous mouse RNF130 (Fig. S6H–L).

Notably, AAV-CRISPR-mediated decreases in *Rnf130* mRNA expression were accompanied by significantly decreased plasma cholesterol levels (Fig. 6C) that was mainly attributable to decreases in the LDL fraction (Fig. S6M). Consistent with previous data in surviving

Author Manuscript Author Manuscript Author Manuscript Author Manuscript

Rnf130$^{-/-}$ mice (Fig. 5), we show increased LDLR protein levels in mice with reduced hepatic *Rnf130* expression (Fig. 6D–E). Taken together, our data show that acute disruption of hepatic *Rnf130* in adult mice results in increased hepatic LDLR protein levels and decreased plasma LDL-C levels.

Silencing endogenous *Rnf130* increases LDLR protein levels and decreases plasma LDL-C levels

The studies described above demonstrate that reducing hepatic *Rnf130* mRNA expression by at least 70% either by gene targeting (Fig. 5) or CRISPR/Cas9 (Fig. 6) is sufficient to increase hepatic LDLR protein levels and lower plasma LDL-C levels in mice. Human and mouse RNF130 protein are highly conserved and share 98% sequence identity suggesting potential conserved function between species. The *RNF130* locus was previously linked with plasma LDL-C levels in a small population (8,090 individuals) of African Americans[33]. To explore whether there were any variants associated with *RNF130* in larger data sets we surveyed multiple summary-level, publicly available association databases, such as UK Biobank (UKBB) and the Global Lipid Genetics Consortium (GLGC)[34,35]. We identified multiple additional variants in the *RNF130* locus that were associated with plasma cholesterol (Fig. S7A). We also asked whether *RNF130* expression was associated with coronary artery disease (CAD) and/or cardiometabolic disease outcomes using the STARNET study (Stockholm-Tartu Atherosclerosis Reverse Networks Engineering Task)[36]. *RNF130* was expressed in a liver gene expression co-regulatory network module that is significantly associated with cardiometabolic outcomes (Fig. S7B). We also found that hepatic *RNF130* expression was significantly elevated in individuals with CAD compared to healthy individuals (p = 7.2e-14). Lastly, we compared these linkage results from human studies with results from a diverse panel of 120 inbred mouse strains known as the Hybrid Mouse Diversity Panel (HMDP). In this panel of mice, we identified significant correlation between hepatic mRNA expression of *Rnf130* and plasma lipid traits including total (Fig. S7C) and LDL (Fig. S7D) cholesterol levels.

To assess the translational potential of our gain- and loss-of-function studies we utilized an antisense oligonucleotide (ASO; Ionis Pharmaceuticals) to silence *Rnf130 in vivo*. Mice were treated twice weekly with either control ASO or RNF130 ASO at a dose of 25 mg/kg for four weeks (Fig. 7A). In contrast to other genetic approaches to disrupt *Rnf130* expression (Fig. 5–6), treatment with *Rnf130* ASO for four weeks reduced hepatic *Rnf130* mRNA levels by more than 90% (Fig. 7B). As we observed in Fig. S5–6, none of the commercially available antibodies were specific for endogenous mouse RNF130 (Fig. S7E–I).

Rnf130 silencing caused significant decreases in total (Fig. 7C), LDL (Fig. 7D–E), and HDL (Fig. 7E, Fig. S7J) cholesterol, with no significant change in plasma TAG, or liver enzymes ALT and AST (Fig. S7K–M). These decreases in plasma LDL-C concentrations were accompanied by significant increases in hepatic LDLR protein levels (Fig. 7F). These data demonstrate that silencing *Rnf130* in adult mice using an ASO compound results in increased LDLR protein levels and lower circulating plasma LDL-C levels.

Author Manuscript Author Manuscript Author Manuscript Author Manuscript

Next, to determine whether these effects on LDL-C were dependent on the availability of LDLR, we repeated our ASO silencing experiment in *Ldlr*$^{-/-}$ mice (Fig. 7G). As observed in wildtype mice treated with *Rnf130* ASO (Fig. 7B), *Rnf130* mRNA expression in ASO treated *Ldlr*$^{-/-}$ mice was decreased by nearly 90% (Fig. 7H). However, silencing *Rnf130* in *Ldlr*$^{-/-}$ mice had no effect on plasma total and LDL-C concentrations (Fig. 7I–J), plasma HDL-C and TAG (Fig. S7N–O), or plasma ALT and AST (Fig. S7P–Q), confirming that the effects on plasma cholesterol observed with silencing *Rnf130* require expression of LDLR.

Discussion

RNF130 is a member of the RING (Really Interesting New Gene) domain family of E3 ubiquitin ligases, which promote the transfer of ubiquitin from ubiquitin-conjugating enzymes (E2s) to lysine residues in target proteins[6]. Furthermore, RNF130 is also part of the unique PA-TM-RING family of RING E3 ubiquitin ligases that contain a transmembrane (TM) domain. Previous studies of other PA-TM-RING ligase family members RNF167 and RNF13 have shown that these ligases are localized to both the plasma membrane and endosomes[7]. It was further shown that this localization dictates target specificity and facilitates endocytic recycling of target proteins. In the present study we show that RNF130 localizes to endosomes and ubiquitinates the LDLR and redistributes LDLR protein away from the plasma membrane. This ubiquitination of LDLR was dependent on both the catalytic RING domain of RNF130, and specific residues in the cytoplasmic tail of LDLR. We utilize mice with gain-of function of RNF130, together with our *in vitro* studies to demonstrate that RNF130 ubiquitinates and redistributes LDLR away from the plasma membrane resulting in decreased levels of cell surface LDLR. We hypothesize that as a result, LDLR-mediated clearance of LDL from the plasma is impaired during RNF130 overexpression leading to elevated plasma LDL-C levels. Using three independent approaches to reduce *Rnf130* expression *in vivo*, we further provide data demonstrating that RNF130 loss-of-function leads to increased LDLR abundance and reduced plasma LDL-C levels.

Earlier studies demonstrated that IDOL, another RING E3 ubiquitin ligase, also ubiquitinates LDLR[21]. Importantly, there are a number of contrasting features between RNF130 and IDOL. RNF130, unlike IDOL, contains a transmembrane domain, restricting its cellular localization. IDOL, however, lacks a TM domain, is cytoplasmic, and contains a FERM binding domain critical for its interaction with LDLR family members. A recent study incorporating a CRISPR screen in human SV589j cells sought to identify regulators of LDL-C movement between the lysosome and endoplasmic reticulum[37]. Of note, this latter study identified disruption of both *RNF130* and *IDOL* as upregulating cell surface levels of LDLR, consistent with RNF130 functioning to regulate LDLR protein levels at the cell surface. In contrast to RNF130, deletion of IDOL in mice had no effect on hepatic LDLR protein or plasma LDL-C levels, although such deletion did have effects on LDL expression in peripheral tissues[38]. Based on these findings and data presented in the current report, we postulate that RNF130 functions by ubiquitinating LDLR at the plasma membrane to signal for receptor internalization, and/or by ubiquitinating endosomal LDLR to prevent recycling to the cell surface. These differences suggest that RNF130 and IDOL may have important, contrasting roles in the regulation of hepatic LDLR and plasma LDL-C.

Author Manuscript Author Manuscript Author Manuscript Author Manuscript

PCSK9 is an important post-translational regulator of LDLR levels that functions to reduce expression of LDLR protein[28,39]. Treatment of hyperlipidemic patients with monoclonal antibodies that target and inactivate PCSK9 results in increased hepatic LDLR expression and significantly reduced plasma LDL-C[40,41]. Our finding that overexpression of RNF130 is able to decrease LDLR levels (and concomitantly increase plasma LDL-C levels) in *Pcsk9*$^{-/-}$ mice suggests that RNF130's effects on LDLR protein are independent of PCSK9.

PCSK9 is known to have a complex reciprocal regulatory relationship with LDLR[27,42]. Studies have shown that PCSK9 is most effective in targeting the LDLR when the LDLR is bound to LDL particles[43,44]. Alternative means of post-translationally increasing the availability of unbound LDLR, such as increased expression of RNF130, are likely to further promote/enhance clearance of LDL-C and are therefore attractive additional therapeutic targets. ASO silencing of *Rnf130* resulted in a 50% decrease in LDL-C, a change comparable to inhibiting PCSK9[40,41], further supporting that RNF130 is a significant regulator of LDLR and LDL-C levels.

Whole body disruption of *Rnf130* expression was incomplete and surviving pups exhibited only a 70% decrease in *Rnf130* mRNA, suggesting that some residual expression of *Rnf130* is necessary for survival. This is in agreement with publicly available human data, in which loss-of-function mutations of the *RNF130* gene are significantly lower than the expected odds. Only nine loss-of-function (LoF) mutations in *RNF130* have been described in the gnomAD database, which is 46% of the expected rate of LoF mutation[45]. Additionally, currently no homozygotes have been identified for these mutations, suggesting that loss of *RNF130* is not well tolerated. Whilst a 70% reduction in *Rnf130* mRNA expression in *Rnf130*$^{-/-}$ mice was sufficient to significantly decrease LDL-C by 45%, the same was not true in heterozygous mice. *Rnf130*$^{+/-}$ mice had only a 30% reduction in *Rnf130* expression, significantly less than the expected 50% reduction, but no significant change in plasma LDL-C. Finally, ASO silencing of *Rnf130*, which induced >90% reduction in hepatic *Rnf130* mRNA levels, elicited the largest decrease in plasma LDL-C levels. The increase in hepatic LDLR and decrease in plasma LDL-C after treatment with ASO is comparable to a recently reported gain-of-function mutation in LDLR[46], which caused a 74% decrease in LDL-C in humans. Taken together, these data suggest that *Rnf130* regulates cholesterol levels in a dose-dependent manner.

Most complex traits, such as coronary artery disease (CAD) and plasma LDL-C, are determined by a number of genetic contributors that each have a modest effect making it difficult to identify genetic variants that increase disease risk, thus hindering the discovery of new drug targets. In fact, genome-wide association study (GWAS) loci only collectively explain approximately 15% of the genetic variance in CAD, suggesting that there are meaningful associations that lie beneath the current genome-wide significance thresholds. Additionally, whilst genome-wide association studies (GWAS) have been a useful tool for identifying regulatory loci, in most cases the molecular link or the specific gene explaining the association between the predicted loci and the disease remains unknown. Our data demonstrating that RNF130 regulates plasma LDL-C and hepatic LDLR availability point to the importance of understanding the molecular mechanisms underlying sub-genome wide significant loci.

Author Manuscript Author Manuscript Author Manuscript Author Manuscript

In conclusion, our data highlight the complex nature of the post-translational regulation of LDLR. We have identified RNF130 as a novel post-translational regulator of hepatic LDLR abundance and activity, that may have important implications for targeting the LDLR pathway to lower plasma LDL-C levels. We further provide pre-clinical evidence that the RNF130-LDLR pathway could be targeted to enhance LDL clearance from the circulation.

Supplementary Material

Refer to Web version on PubMed Central for supplementary material.

Acknowledgements

We thank Ionis Pharmaceuticals for providing antisense oligonucleotide compounds. We thank all members of the Tarling-Vallim and Tontonoz labs at UCLA for advice, discussion, and sharing reagents.

Sources of Funding

B.L.C. was sponsored by an AHA post-doctoral fellowship (19POST34380145). K.E.J. was sponsored by the UCLA Vascular Biology T32 fellowship (5T32HL069766). M.S. is funded by NIH grant HL138193. A.B. is funded by NIH grants DK125048 and HL107794. T.Q. de A.V. is funded by NIH grant DK118064. E.J.T. is funded by NIH grant HL136543. E.J.T. and T.Q. de A.V. are funded by NIH grant DK128952.

Non-standard Abbreviations and Acronyms

AAV	Adeno-associated virus
CLiP	On-Column Lipoprotein Profile
CRISPR	Clustered Regularly Interspaced Short Palindromic Repeats
RING	Really Interesting New Gene
RNF130	Ring Finger containing protein 130
TMD	Transmembrane domain

References

1. Benjamin EJ, Muntner P, Alonso A, Bittencourt MS, Callaway CW, Carson AP, Chamberlain AM, Chang AR, Cheng S, Das SR, et al. Heart Disease and Stroke Statistics—2019 Update: A Report From the American Heart Association. Circulation. 2019;139:e56–e66. [PubMed: 30700139]
2. Wang Y, Huang Y, Hobbs HH, Cohen JC. Molecular characterization of proprotein convertase subtilisin/kexin type 9-mediated degradation of the LDLR. J Lipid Res. 2012;53:1932–43. [PubMed: 22764087]
3. Goldstein JL, Brown MS. The low-density lipoprotein pathway and its relation to atherosclerosis. Annu Rev Biochem. 1977;46:897–930. [PubMed: 197883]
4. Goldstein JL, Brown MS. History of Discovery : The LDL Receptor. Arterioscler Thromb. 2010;29:431–438.
5. Buetow L, Huang DT. Structural insights into the catalysis and regulation of E3 ubiquitin ligases. Nat Rev Mol Cell Biol. 2016;17:626–642. [PubMed: 27485899]
6. Deshaies RJ, Joazeiro CAP. RING Domain E3 Ubiquitin Ligases. Annu Rev Biochem. 2009;78:399–434. [PubMed: 19489725]

Author Manuscript Author Manuscript Author Manuscript Author Manuscript

7. Yamazaki Y, Schönherr C, Varshney GK, Dogru M, Hallberg B, Palmer RH. Goliath family E3 ligases regulate the recycling endosome pathway via VAMP3 ubiquitylation. EMBO J. 2013;32:524–537. [PubMed: 23353890]
8. Guais A, Siegrist S, Solhonne B, Jouault H, Guellaën G, Bulle F. h-Goliath, paralog of GRAIL, is a new E3 ligase protein, expressed in human leukocytes. Gene. 2006;112–120.
9. Guais A, Solhonne B, Melaine N, Guellaën G, Bulle F. Goliath, a Ring-H2 Mitochondrial Protein, Regulated by Luteinizing Hormone/Human Chorionic Gonadotropin in Rat Leydig Cells1. Biol Reprod. 2004;70:204–213. [PubMed: 13679316]
10. Nakamura N. The role of the transmembrane RING finger proteins in cellular and organelle function. Membranes. 2011;1:354–393. [PubMed: 24957874]
11. Koo BK, Spit M, Jordens I, Low TY, Stange DE, Van De Wetering M, Van Es JH, Mohammed S, Heck AJR, Maurice MM, et al. Tumour suppressor RNF43 is a stem-cell E3 ligase that induces endocytosis of Wnt receptors. Nature. 2012;488:665–669. [PubMed: 22895187]
12. Lin H, Li S, Shu HB. The Membrane-Associated MARCH E3 Ligase Family: Emerging Roles in Immune Regulation. Front Immunol. 2019;10:1751. [PubMed: 31404274]
13. Ulrich HD. Protein-protein interactions within an E2-RING finger complex: Implications for ubiquitin-dependent DNA damage repair. J Biol Chem. 2003;278:7051–7058. [PubMed: 12496280]
14. Davidoff AM, Ng CYC, Zhou J, Spence Y, Nathwani AC. Sex significantly influences transduction of murine liver by recombinant adeno-associated viral vectors through an androgen-dependent pathway. Blood. 2003;102:480–488. [PubMed: 12637328]
15. Xiao X, Li J, Samulski RJ. Production of High-Titer Recombinant Adeno-Associated Virus Vectors in the Absence of Helper Adenovirus. J Virol. 1998;72:2224–2232. [PubMed: 9499080]
16. Jarrett KE, Lee C, De Giorgi M, Hurley A, Gillard BK, Doerfler AM, Li A, Pownall HJ, Bao G, Lagor WR. Somatic Editing of Ldlr With Adeno-Associated Viral-CRISPR Is an Efficient Tool for Atherosclerosis Research. Arterioscler Thromb Vasc Biol. 2018;38:1997–2006. [PubMed: 30026278]
17. Warnick GR, Albers JJ. A comprehensive evaluation of the heparin-manganese precipitation procedure for estimating high density lipoprotein cholesterol. J Lipid Res. 1978;19:65–76. [PubMed: 202660]
18. Garber DW, Kulkarni KR, Anantharamaiah GM. A sensitive and convenient method for lipoprotein profile analysis of individual mouse plasma samples. J Lipid Res. 2000;41:1020–1026. [PubMed: 10828095]
19. Rajamoorthi A, Lee RG, Baldán Á. Therapeutic silencing of FSP27 reduces the progression of atherosclerosis in Ldlr–/– mice. Atherosclerosis. 2018;275:43–49. [PubMed: 29859472]
20. Calkin AC, Goult BT, Zhang L, Fairall L, Hong C, Schwabe JWR, Tontonoz P. FERM-dependent E3 ligase recognition is a conserved mechanism for targeted degradation of lipoprotein receptors. Proc Natl Acad Sci U S A. 2011;108:20107–20112. [PubMed: 22109552]
21. Zelcer N, Hong C, Boyadjian R, Tontonoz P, Mev S. LXR Regulates Cholesterol Uptake through Idol-dependent Ubiquitination of the LDL Receptor. Life Sci. 2009;325:100–104.
22. Cradick TJ, Qiu P, Lee CM, Fine EJ, Bao G. COSMID: A web-based tool for identifying and validating CRISPR/Cas off-target sites. Mol Ther - Nucleic Acids. 2014;3:e214. [PubMed: 25462530]
23. Li A, Lee CM, Hurley AE, Jarrett KE, De Giorgi M, Lu W, Balderrama KS, Doerfler AM, Deshmukh H, Ray A, et al. A Self-Deleting AAV-CRISPR System for In Vivo Genome Editing. Mol Ther - Methods Clin Dev. 2019;12:111–122. [PubMed: 30619914]
24. Zheng N, Wang P, Jeffrey PD, Pavletich NP. Structure of a c-Cbl-UbcH7 complex: RING domain function in ubiquitin-protein ligases. Cell. 2000;102:533–539. [PubMed: 10966114]
25. Chen WJ, Goldstein JL, Brown MS. NPXY, a sequence often found in cytoplasmic tails, is required for coated pit-mediated internalization of the low density lipoprotein receptor. J Biol Chem. 1990;265:3116–3123. [PubMed: 1968060]
26. Galan J-M, Haguenauer-Tsapis R Ubiquitin Lys63 is involved in ubiquitination of a yeast plasma membrane protein. EMBO J. 1997;16:5847–5854. [PubMed: 9312043]

Author Manuscript Author Manuscript Author Manuscript Author Manuscript

27. Tavori H, Fan D, Blakemore JL, Yancey PG, Ding L, Linton S, Fazio S. Serum proprotein convertase subtilisin/kexin type 9 and cell surface low-density lipoprotein receptor: evidence for a reciprocal regulation. 2014;127:2403–2413.

28. Lagace TA, Curtis DE, Garuti R, McNutt MC, Sahng WP, Prather HB, Anderson NN, Ho YK, Hammer RE, Horton JD. Secreted PCSK9 decreases the number of LDL receptors in hepatocytes and in livers of parabiotic mice. J Clin Invest. 2006;116:2995–3005. [PubMed: 17080197]

29. Sahng WP, Moon YA, Horton JD. Post-transcriptional regulation of low density lipoprotein receptor protein by proprotein convertase subtilisin/kexin type 9a in mouse liver. J Biol Chem. 2004;279:50630–50638. [PubMed: 15385538]

30. Coleman JLJ, Brennan K, Ngo T, Balaji P, Graham RM, Smith NJ. Rapid Knockout and Reporter Mouse Line Generation and Breeding Colony Establishment Using EUCOMM Conditional-Ready Embryonic Stem Cells: A Case Study. Front Endocrinol. 2015;6:105.

31. Zincarelli C, Soltys S, Rengo G, Rabinowitz JE. Analysis of AAV serotypes 1–9 mediated gene expression and tropism in mice after systemic injection. Mol Ther. 2008;16:1073–1080. [PubMed: 18414476]

32. Pañeda A, Vanrell L, Mauleon I, Crettaz JS, Berraondo P, Timmermans EJ, Beattie SG, Twisk J, Van Deventer S, Prieto J, et al. Effect of adeno-associated virus serotype and genomic structure on liver transduction and biodistribution in mice of both genders. Hum Gene Ther. 2009;20:908–917. [PubMed: 19419275]

33. Lettre G, Palmer CD, Young T, Ejebe KG, Allayee H, Benjamin EJ, Bennett F, Bowden DW, Chakravarti A, Dreisbach A, et al. Genome-Wide association study of coronary heart disease and its risk factors in 8,090 african americans: The nhlbi CARe project. PLoS Genet. 2011;

34. Klarin D, Damrauer SM, Cho K, Sun YV, Teslovich TM, Honerlaw J, Gagnon DR, DuVall SL, Li J, Peloso GM, et al. Genetics of blood lipids among ~300,000 multi-ethnic participants of the Million Veteran Program. Nat Genet. 2018;50:1514–1523. [PubMed: 30275531]

35. Liu DJ, Peloso GM, Yu H, Butterworth AS, Wang X, Mahajan A, Saleheen D, Emdin C, Alam D, Alves AC, et al. Exome-wide association study of plasma lipids in >300,000 individuals. Nat Genet. 2017;49:1758–1766. [PubMed: 29083408]

36. Koplev S, Seldin M, Sukhavasi K, Ermel R, Pang S, Zeng L, Bankier S, Di Narzo A, Cheng H, Meda V, et al. A mechanistic framework for cardiometabolic and coronary artery diseases. Nat Cardiovasc Res. 2022;1:85–100. [PubMed: 36276926]

37. Trinh MN, Brown MS, Goldstein JL, Han J, Vale G, McDonald JG, Seemann J, Mendell JT, Lu F. Last step in the path of LDL cholesterol from lysosome to plasma membrane to ER is governed by phosphatidylserine. Proc Natl Acad Sci U S A. 2020;117:18521–18529. [PubMed: 32690708]

38. Hong C, Marshall SM, McDaniel AL, Graham M, Layne JD, Cai L, Scotti E, Boyadjian R, Kim J, Chamberlain BT, et al. The LXR-idol axis differentially regulates plasma LDL levels in primates and mice. Cell Metab. 2014;20:910–918. [PubMed: 25440061]

39. Horton JD, Shah NA, Warrington JA, Anderson NN, Park SW, Brown MS, Goldstein JL. Combined analysis of oligonucleotide microarray data from transgenic and knockout mice identifies direct SREBP target genes. Proc Natl Acad Sci U S A. 2003;100:12027–32. [PubMed: 14512514]

40. Stein EA, Mellis S, Yancopoulos GD, Stahl N, Logan D, Smith WB, Lisbon E, Gutierrez M, Webb C, Wu R, et al. Effect of a monoclonal antibody to PCSK9 on LDL cholesterol. Obstet Gynecol Surv. 2012;67:413–414.

41. Blom DJ, Hala T, Bolognese M, Lillestol MJ, Toth PD, Burgess L, Ceska R, Roth E, Koren MJ, Ballantyne CM, et al. A 52-week placebo-controlled trial of evolocumab in hyperlipidemia. N Engl J Med. 2014;370:1809–1819. [PubMed: 24678979]

42. Mousavi SA, Berge KE, Berg T, Leren TP. Affinity and kinetics of proprotein convertase subtilisin/kexin type 9 binding to low-density lipoprotein receptors on HepG2 cells. FEBS J. 2011;278:2938–2950. [PubMed: 21692990]

43. Fazio S, Minnier J, Shapiro MD, Tsimikas S, Tarugi P, Averna MR, Arca M, Tavori H. Threshold Effects of Circulating Angiopoietin-Like 3 Levels on Plasma Lipoproteins. J Clin Endocrinol Metab. 2017;102:3340–3348. [PubMed: 28633452]

Author Manuscript Author Manuscript Author Manuscript Author Manuscript

44. Shapiro MD, Tavori H, Fazio S. PCSK9 from basic science discoveries to clinical trials. Circ Res. 2018;122:1420–1438. [PubMed: 29748367]

45. Karczewski KJ, Francioli LC, Tiao G, Cummings BB, Alföldi J, Wang Q, Collins RL, Laricchia KM, Ganna A, Birnbaum DP, et al. The mutational constraint spectrum quantified from variation in 141,456 humans. bioRxiv. 2020;531210.

46. Björnsson E, Gunnarsdóttir K, Halldórsson GH, Sigurðsson Á, Árnadóttir GA, Jónsson H, Ólafsdóttir EF, Niehus S, Kehr B, Sveinbjörnsson G, et al. Lifelong Reduction in LDL Cholesterol Due to a Gain-of-Function Mutation in LDLR. Circ Genomic Precis Med. 2020;CIRCGEN.120.003029.

Author Manuscript Author Manuscript Author Manuscript Author Manuscript

Novelty and Significance

What is known?

- RNF130 is a member of the unique membrane-bound protease-associated domain-containing E3 ubiquitin ligases.
- RNF130 has no known molecular targets.
- The Low-density lipoprotein receptor (LDLR) is the major determinant of plasma LDL cholesterol (LDL-C) levels and is the target of many therapeutic interventions to lower circulating plasma cholesterol levels.

What new information does this article contribute?

- We identify the LDLR as the first known target of the E3 ubiquitin ligase RNF130.
- RNF130-mediated ubiquitination of LDLR results in receptor redistribution away from the plasma membrane.
- Our study defines the molecular mechanism that explains previously observed associations between variants in the *RNF130* locus and plasma LDL-C levels.

Author Manuscript Author Manuscript Author Manuscript Author Manuscript

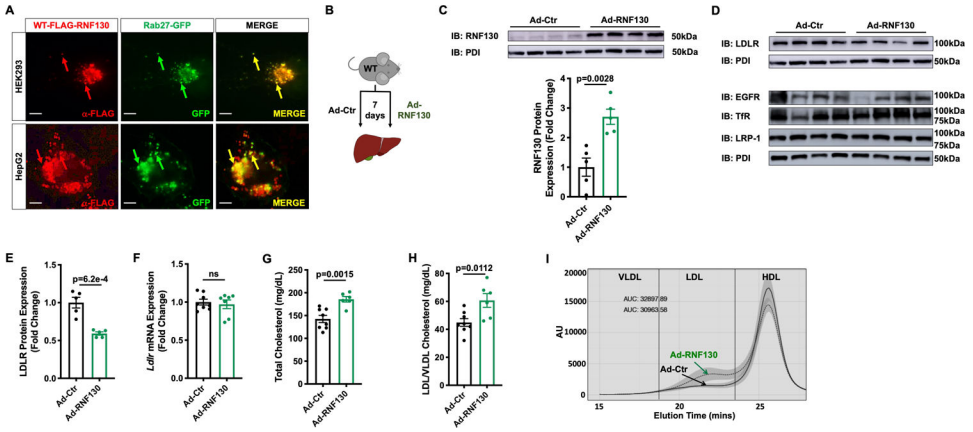

Figure 1. RNF130 expression reduces hepatic LDLR and increases plasma LDL-C level.

(A) Immunofluorescence images of HEK293 and HepG2 cells co-transfected with WT-FLAG-RNF130 and either control plasmid or Rab27a-GFP (pan-endosomal marker). Original magnification 63X. Arrows indicate co-localization. Scale bar indicates 50mm. **(B)** Experimental design: WT mice were treated once on day 0 with control adenovirus (Ad-Ctr) or adenovirus overexpressing human RNF130 (Ad-RNF130) and tissues harvested 7 days later. **(C)** Hepatic protein expression and accompanying densitometry of RNF130 in mice treated as in (B) (Ad-Ctr n=5 and Ad-RNF130 n=5). **(D)** Hepatic protein expression of endocytosed receptors in mice treated as in (B) (Ad-Ctr n=5 and Ad-RNF130 n=5; individual dots represent individual animals). **(E)** Quantification of hepatic LDLR protein from (D) (Ad-Ctr n=5 and Ad-RNF130 n=5). **(F)** Hepatic mRNA expression of LDLR from mice treated as in (B) (Ad-Ctr n=8 and Ad-RNF130 n=7; individual dots represent individual animals). **(G-H)** Plasma total cholesterol **(G)** and LDL (LDL/VLDL) cholesterol **(H)** in WT mice treated as in (B) (Ad-Ctr n=8 and Ad-RNF130 n=6; individual dots represent individual animals). **(I)** FPLC lipoprotein profiles in WT mice treated as in (B). Data are expressed as mean ±SEM. FPLC lipoprotein profiles are plotted as mean absorbance unit (AU) ±SEM (Ad-Ctr n=8 and Ad-RNF130 n=6). *P* values were determined by (C, E-H) Student's *t*-test. ns, not significant. Ad, adenovirus; AU, absorbance unit; Ctr, Control; EGFR, epidermal growth factor receptor; HDL, high-density lipoprotein; IB, immunoblot; LDL, low-density lipoprotein; LDLR, LDL receptor; LRP-1, LDLR-related protein 1; PDI, protein disulfide isomerase; TfR, transferrin receptor; VLDL, very low-density lipoprotein.

Author Manuscript Author Manuscript Author Manuscript Author Manuscript

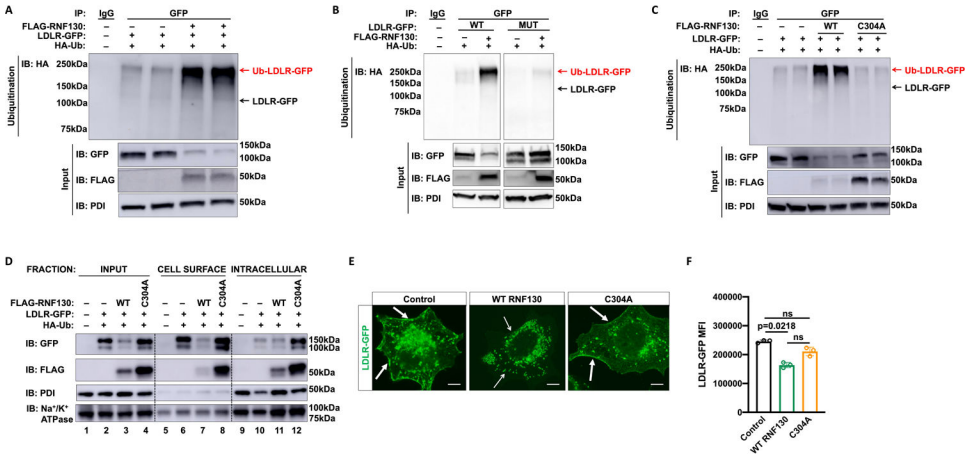

Figure 2. RNF130 is a RING-dependent E3 ligase that ubiquitinates LDLR and redistributes LDLR away from the plasma membrane.

(A) HEK293 cells were co-transfected with LDLR-GFP, FLAG-RNF130, and HA-Ubiquitin expression plasmids. After 36 hours, lysates were subjected to immunoprecipitation (IP) with anti-GFP and immunoblotting (IB) with anti-HA to detect ubiquitinated proteins (upper panel). Total cell lysates (input; lower panels) were processed for western blotting with antibodies to anti-GFP, anti-FLAG, or anti-PDI. **(B)** HEK293 cells were co-transfected with wildtype (WT) or mutant (MUT) LDLR-GFP (K811/816/830RC839A), FLAG-RNF130, and HA-Ubiquitin. After 36 hours, lysates were subjected to IP and IB as in (A). **(C)** HEK293 cells were co-transfected with LDLR-GFP, wildtype (WT) FLAG-RNF130 or mutant FLAG-RNF130 (C304A) and HA-Ubiquitin expression plasmids. After 36 hours, lysates were subjected to IP and IB as in (A). **(D)** HEK293 cells were co-transfected with LDLR-GFP, wildtype (WT) FLAG-RNF130 or mutant FLAG-RNF130 (C304A) and HA-Ubiquitin expression plasmids. After 36 hours, cells were incubated with biotin at 4°C to label cell surface proteins. Total cell lysates (input; lanes 1–4), biotinylated proteins (membrane; lanes 5–8), and unmodified proteins (intracellular; lanes 9–12) were processed for western blotting with antibodies to anti-GFP, anti-FLAG, anti-PDI (intracellular) and anti-Na^+/K^+ ATPase (plasma membrane). **(E)** Immunofluorescence images of HEK293 cells co-transfected with LDLR-GFP and either wildtype (WT) FLAG-RNF130 or mutant FLAG-RNF130 (C304A) Original magnification 63X. White arrows indicate plasma membrane. Scale bars indicate 50mm. **(F)** Mean fluorescence intensity (MFI) of LDLR-GFP quantification of confocal images in (E). n=3 images from 3 independent transfections. *P* values were determined by Kruskal-Wallis test with Dunn correction. GFP, green fluorescent protein; HA, haemagglutinin; IB, immunoblot; IP, immunoprecipitation; MFI, mean fluorescence intensity; PDI, protein disulfide isomerase; Ub, ubiquitin.

Author Manuscript Author Manuscript Author Manuscript Author Manuscript

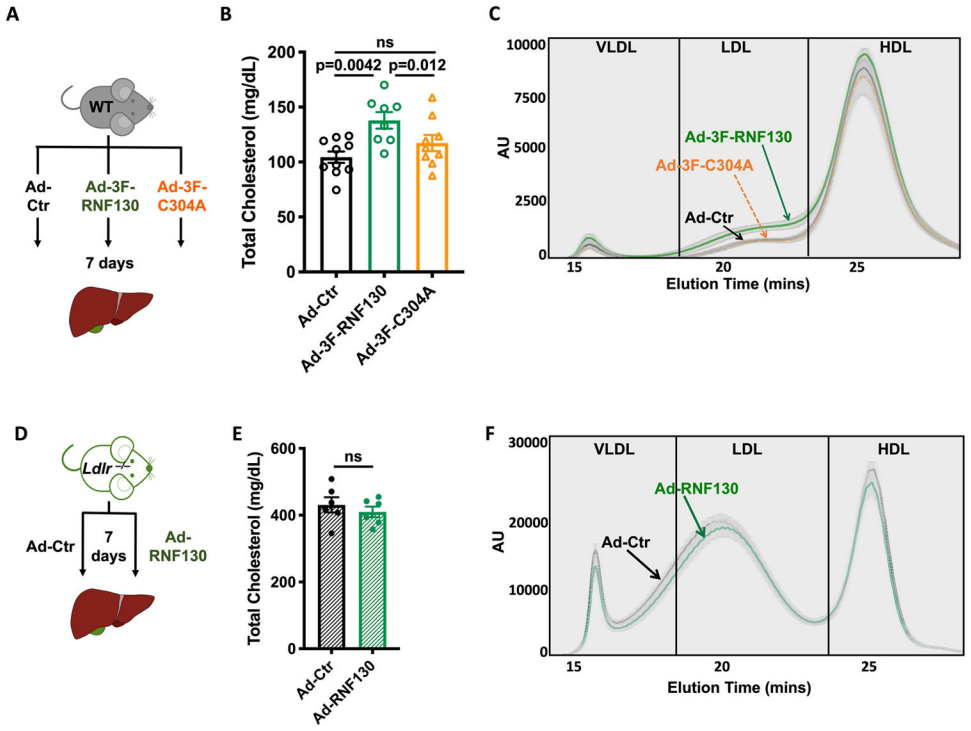

Figure 3. RNF130 increases plasma LDL-C levels *in vivo* in a process that is dependent on LDLR and RNF130 E3 ligase activity.

(A) Experiment design: Wildtype (WT) mice were treated once on day 0 with control adenovirus (Ad-Ctr), or adenovirus overexpressing human RNF130 with an N-terminal 3xFLAG epitope tag (Ad-3F-RNF130) or 3F-RNF130 with a single point mutation in the RING domain (Ad-3F-C304A) and tissues harvested 7 days later. **(B)** Plasma total cholesterol in WT mice treated as in (A) (Ad-Ctr n=10, Ad-3F-RNF130 n=8, Ad-3F-C304A n=9; individual dots represent individual animals). **(C)** FPLC lipoprotein profiles in WT mice treated as in (A). FPLC lipoprotein profiles are plotted as mean absorbance unit (AU) ±SEM (Ad-Ctr n=10, Ad-3F-RNF130 n=8, Ad-3F-C304A n=9). **(D)** Experimental design: *Ldlr*$^{-/-}$ mice were treated once on day 0 with control adenovirus (Ad-Ctr) or adenovirus overexpressing human RNF130 (Ad-RNF130) and tissues harvested 7 days later. **(E)** Plasma total cholesterol in WT mice treated as in (D) (Ad-Ctr n=6, Ad-RNF130 n=6; individual dots represent individual animals). **(F)** FPLC lipoprotein profiles in WT mice treated as in (D). FPLC lipoprotein profiles are plotted as mean absorbance unit (AU) ±SEM (Ad-Ctr n=6, Ad-RNF130 n=6). Data are expressed as mean ±SEM. *P* values were determined by Kruskal-Wallis test with Dunn correction (B) or Student's *t* test (E). ns, not significant. Ad, adenovirus; AU, absorbance unit; Ctr, Control; HDL, high-density lipoprotein; LDL, low-density lipoprotein; LDLR, LDL receptor; VLDL, very low-density lipoprotein; WT, wildtype; 3F, 3-FLAG.

Author Manuscript Author Manuscript Author Manuscript Author Manuscript

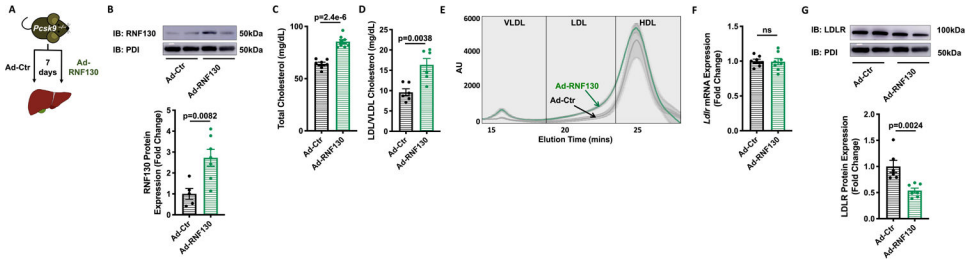

Figure 4. RNF130-mediated regulation of plasma LDL-C depends on hepatic LDLR abundance.

(A) Experiment design: *Pcsk9*$^{-/-}$ mice were treated once on day 0 with control adenovirus (Ad-Ctr) or adenovirus overexpressing human RNF130 (Ad-RNF130) and tissues harvested 7 days later. **(B)** Hepatic protein expression of representative animals and accompanying densitometry of RNF130 in *Pcsk9*$^{-/-}$ mice treated with Ad-Ctr or Ad-RNF130 (Ad-Ctr n=5, Ad-RNF130 n=7; individual dots represent quantification of individual animals analyzed by western blot). **(C-D)** Plasma total cholesterol **(C)** and LDL (LDL/VLDL) cholesterol **(D)** in *Pcsk9*$^{-/-}$ mice treated with Ad-Ctr (n=7) or Ad-RNF130 (n=8). Individual dots represent individual animals. **(E)** FPLC lipoprotein profiles in *Pcsk9*$^{-/-}$ mice treated with Ad-Ctr (n=7) or Ad-RNF130 (n=8). FPLC lipoprotein profiles are plotted as mean absorbance unit (AU) ±SEM. **(F)** Hepatic *Ldlr* mRNA expression in *Pcsk9*$^{-/-}$ mice treated with Ad-Ctr (n=6) or Ad-RNF130 (n=8). Individual dots represent individual animals. **(G)** Hepatic LDLR protein expression from representative animals and accompanying densitometry in *Pcsk9*$^{-/-}$ mice treated with Ad-Ctr (n=6) or Ad-RNF130 (n=7). Individual dots represent quantification of individual animals analyzed by western blot. Data are expressed as mean ±SEM. *P* values were determined by Mann-Whitney U-test (B) or Student's *t* test (C-D, F-G). ns, not significant. Ad, adenovirus; AU, absorbance unit; Ctr, Control; HDL, high-density lipoprotein; IB, immunoblot; LDL, low-density lipoprotein; LDLR, LDL receptor; Pcsk9, proprotein convertase subtilisin kinase 9; PDI, protein disulfide isomerase; VLDL, very low-density lipoprotein.

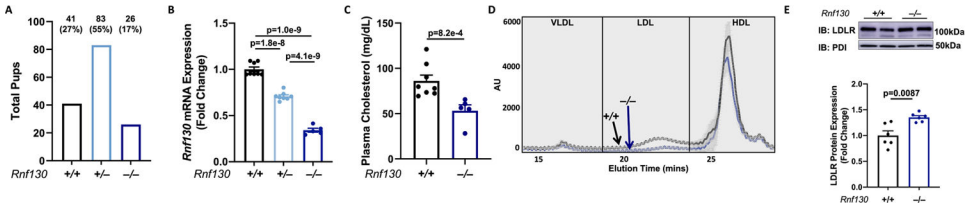

Figure 5. Partial knockout of *Rnf130* results in decreased plasma LDL-C.

(A) Total number of pups obtained for each genotype from heterozygous breedings showing that homozygous nulls (–/–) are obtained at less than the expected mendelian ratio (n=35 litters, 204 pups total, mean litter size 5.8). **(B)** Hepatic mRNA expression of *Rnf130* in 10-week old $Rnf130^{+/+}$ (n=11), $Rnf130^{+/-}$ (n=8), and $Rnf130^{-/-}$ (n=5) mice. Individual dots represent individual animals. **(C)** Total plasma cholesterol in 10-week old $Rnf130^{+/+}$ (n=8) and $Rnf130^{-/-}$ (n=5) mice. Individual dots represent individual animals. **(D)** FPLC lipoprotein profiles of 10-week old $Rnf130^{+/+}$ (n=8) and $Rnf130^{-/-}$ (n=5) mice. Data are expressed as mean ±SEM. FPLC lipoprotein profiles are plotted as mean absorbance unit (AU) ±SEM. **(E)** Representative western blot and accompanying densitometry of hepatic protein expression of LDLR in $Rnf130^{+/+}$ (n=6) and $Rnf130^{-/-}$ (n=6) mice. Individual dots represent quantification of individual animals analyzed by western blot. *P* values were determined by Kruskal-Wallis with Dunn's correction (B) or Mann-Whitney U-test (C,E). ns, not significant. AU, absorbance unit; HDL, high-density lipoprotein; LDL, low-density lipoprotein; VLDL, very low-density lipoprotein; +/+, wildtype; –/–, knockout.

Author Manuscript Author Manuscript Author Manuscript Author Manuscript

Author Manuscript Author Manuscript Author Manuscript Author Manuscript

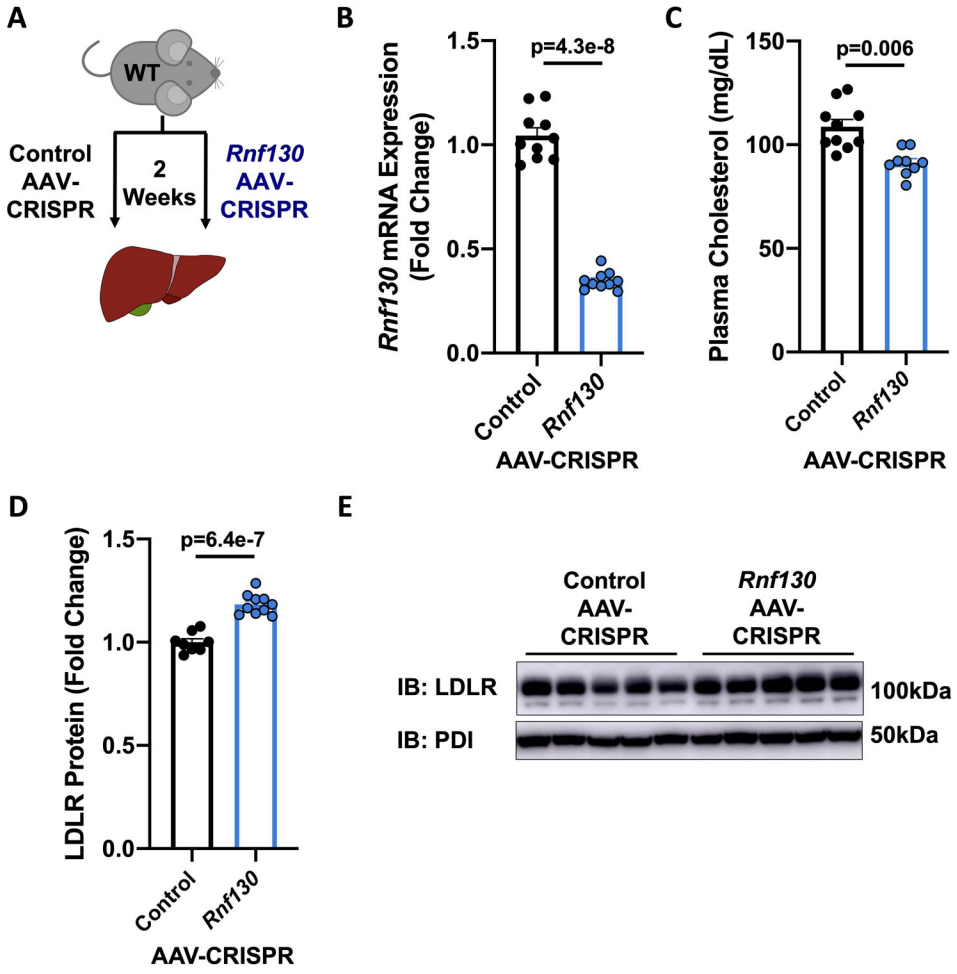

Figure 6. Liver-specific disruption of *Rnf130* reduces plasma cholesterol levels.

(A) C57BL/6 wildtype (WT) mice were treated with 5×10^{11} genome copies of Control AAV-CRISPR (n=10) or *Rnf130* AAV-CRISPR (n=10) for 2 weeks. **(B)** Hepatic *Rnf130* mRNA expression in WT mice treated as in (A). Individual dots represent individual animals. **(C)** Plasma total cholesterol in WT mice treated as in (A). Individual dots represent individual animals. **(D, E)** Hepatic LDLR protein expression and accompanying densitometry of mice treated as in (A). **(D)** Individual dots represent quantification of individual animals analyzed by western blot. Data are expressed as mean ±SEM. *P* values were determined by Student's *t*-test (B-D). AAV, adeno-associated virus; IB, immunoblot; LDLR, low-density lipoprotein receptor; PDI, protein disulfide isomerase.

Author Manuscript Author Manuscript Author Manuscript Author Manuscript

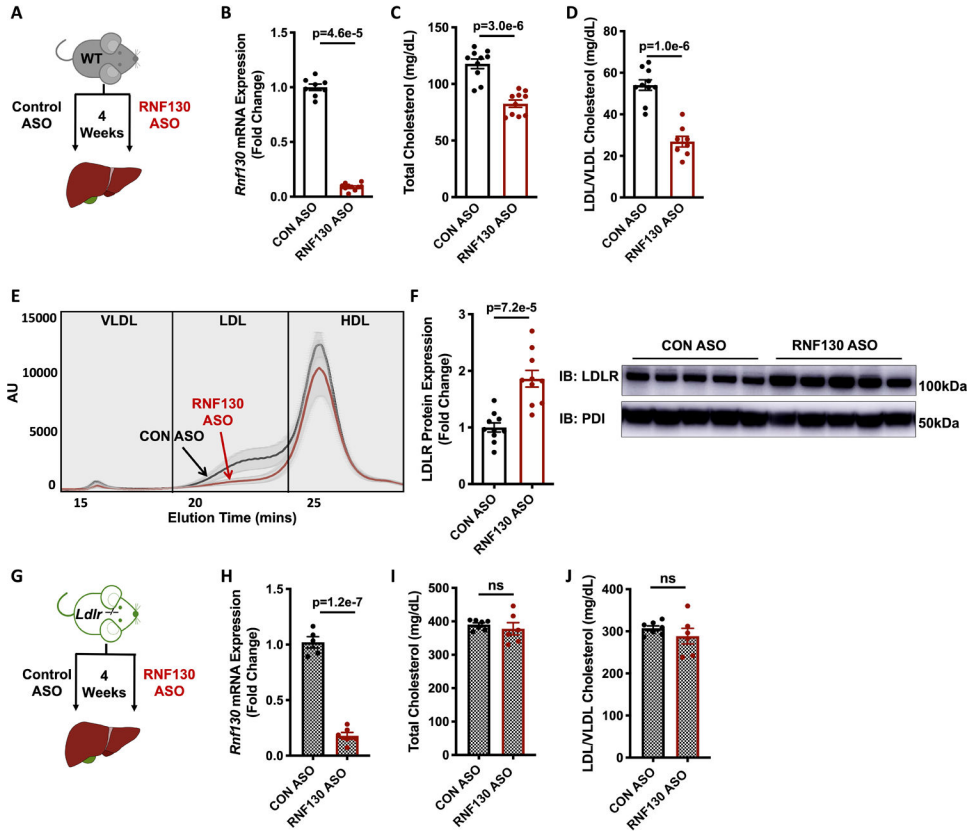

Figure 7. Antisense oligonucleotide treatment to silence hepatic *Rnf130* increases hepatic LDLR and decreases plasma cholesterol levels.

(A) C57BL/6 wildtype (WT) mice were treated with Control or RNF130 antisense oligonucleotide (ASO) for 4 weeks. **(B)** Hepatic mRNA expression of *Rnf130* in WT mice treated with Control ASO (n=10) or RNF130 ASO (n=10) as in (A). Individual dots represent individual animals. **(C-E)** Plasma total cholesterol **(C)**, LDL (LDL/VLDL) cholesterol **(D)**, and FPLC lipoprotein profiles **(E)** in WT mice treated as in (A). **(C-D)** Individual dots represent individual animals. **(F)** Hepatic LDLR protein expression and accompanying densitometry in WT mice treated as in (A). **(G)** *Ldlr*$^{-/-}$ mice were treated with RNF130 ASO for 4 weeks. **(H)** Hepatic *Rnf130* mRNA expression in *Ldlr*$^{-/-}$ mice treated with Control ASO (n=7) or RNF130 ASO (n=6) as in (G). Individual dots represent individual animals. **(I-J)** Plasma total cholesterol **(I)** and LDL (LDL/VLDL) cholesterol **(J)** in *Ldlr*$^{-/-}$ mice treated as in (G). Individual dots represent individual animals. Data are expressed as mean ±SEM. FPLC lipoprotein profiles are plotted as mean absorbance unit (AU) ±SEM (Control ASO n=10 and RNF130 ASO n=10). *P* values were determined by Student's *t*-test (B-D,F,H-J). ns, not significant. ASO, antisense oligonucleotide; AU, absorbance unit; CON, Control; HDL, high-density lipoprotein; IB, immunoblot; LDL, low-density lipoprotein; LDLR, LDL receptor; PDI, protein disulfide isomerase; VLDL, very low-density lipoprotein.